Vulnerability Assessment for Wireless Mesh Networks Under Probabilistic Region Failure Model

Jiajia Liu, *Non-Member, IEEE,* Xiaohong Jiang, *Senior Member, IEEE,* Hiroki Nishiyama, *Member, IEEE,* and Nei Kato, *Senior Member, IEEE*

Abstract—Wireless networks in open environment are exposed to various large region threats, like the natural disasters and malicious attacks. Available work regarding region failures generally adopt a kind of "deterministic" failure models, which failed to reflect some key features of a real region failure. In this paper, we provide a more general "probabilistic" region failure model to capture the key features of a region failure and apply it for the vulnerability assessment of wireless mesh networks. To facilitate such assessment, we develop a grid partition-based scheme to estimate the expected flow capacity degradation from a random region failure. We then establish a theoretical framework to determine a suitable grid partition such that a specified estimation error requirement is satisfied. The grid partition technique is also useful for identifying the vulnerable zones of a network, which can guide network designers to initiate proper network protection against such failures. The work in this paper helps us understand the network vulnerability under a region failure, and can facilitate the design and maintenance of future highly survivable wireless networks.

Index Terms—Wireless mesh networks, region failure, network vulnerability.

I. INTRODUCTION

In recent years, the wireless mesh networks have increasingly gained interests in both academia and industry. As a promising and flexible networking technology, the wireless mesh networks are expected to support data communications for some important and mission critical applications, like the disaster relief and battlefield headquarter construction. Due to the nature of wireless communications, the nodes there are exposed to various hazards [1]–[3], such as the natural disasters and malicious network attacks [4], [5]. Thus, the pre-active evaluation of network vulnerability and survivability against network failures becomes essential for the design and maintenance of future highly survivable wireless mesh networks.

In the light of failure inevitability and its detrimental consequences, many studies have been dedicated to the design of failure-resilient networks. Stefanakos *et al.* examined the routing issue in networks that require guaranteed reliability against multiple link failures in [6]. In [7] Awerbuch *et al.* proposed an on-demand routing protocol for ad hoc wireless networks, which provides resilience to byzantine failures caused by individual or colluding nodes. In [8] Bhandari

J. Liu, H. Nishiyama and N. Kato are with the Graduate School of Information Sciences, Tohoku University, Aobayama 6-3-09, Sendai, 980-8579, JAPAN. E-mail: {liu-jia,kato}@it.ecei.tohoku.ac.jp.

X. Jiang is with the School of Systems Information Science, Future University Hakodate, Kamedanakano 116-2, Hakodate, Hokkaido, 041-8655, JAPAN. E-mail: jiang@fun.ac.jp.

and Vaidya considered the problem of reliable broadcast in a wireless network where each node can fail independently. In [9] Yu and Zhang proposed R-Sentry, a novel scheduling algorithm for sensor networks that attempts to bound the service loss duration due to node failures and provides continuous surveillance coverage even when a subset of sensors fail. The fast restoration and protection against link and node failures have also been explored recently, see, for example [10]–[13].

Most of available network survivability studies are based on one common assumption: failures are random and independent, which failed to reflect many real scenarios. The real-world disasters or attacks, like the earthquake, hurricane, physical bomb explosion or electromagnetic pulse (EMP) attack [14], [15], always happen in a particular geographical location and result in the so-called *region failure* ([16], [17]). Under a region failure, multiple network components may simultaneously corrupt but they are geographically correlated and constrained within a specific region. Thus, it is important to take into account the geographical information of networks in the study of such failures, and some research has been conducted to understand the impact of region failures on wired backbone networks ([17]–[19]). In this paper, we focus on the vulnerability assessment of wireless mesh networks under a random region failure.

There are few related works considering region failures inside wireless networks. Sen *et al.* explored the region-based connectivity issue in wireless networks and showed how to adjust the transmitting power to maintain a region-based connectivity in presence of region failures [16], [20]. This work was further extended into multiple region failure model (MRFM) [21], where the failures are no longer confined within a single region. In [22] Xu *et al.* adopted the percolation theory to characterize the spread of correlated failures in large wireless networks, and analyzed the condition under which an initial node failure will/will not permeate the whole network. Azimi *et al.* in [23] addressed the problem of building data redundancy with the minimum communication cost in a sensor network, where many nodes may simultaneously fail due to a bomb attack or river overflow.

It is notable that the region failure models adopted in previous region failure-related studies (for both wired and wireless networks) can be regarded as a kind of "deterministic" failure models, like the single circular model in [16], [18], [20], [21], [23], and line cut model in [17]–[19], where any network component intersecting with the concerned failure region will always be destroyed (i.e., destroyed with probability 1). These "deterministic" failure models, although

simple and easy to use, neglected two key facts of real-world region failures: network components can only be destroyed with certain probability (not always probability 1), and more importantly, such failure probability of a network component tends to monotonously decrease as it is farther away from the region center. Based on this observation, we believe a "probabilistic" model addressing these two key features will be much more suitable for network vulnerability study. In this paper, we consider such a probabilistic failure model and apply it to assess the vulnerability of wireless mesh networks. The main contributions of this paper are as follows:

- We provide a general and more realistic probabilistic region failure model to capture the key features of region failures, which covers the deterministic failure models in [16], [18] as special cases.
- Based on the new failure model, we formulate the expected flow capacity degradation problem in wireless mesh networks as a network zone partition problem, which is hard to solve for a large network. We then develop a grid partition scheme to efficiently estimate the expected flow capacity degradation from a random region failure. The grid partition technique can also help us to identify the vulnerable zones of a network.
- A theoretical framework is further established to analyze the estimation error from using the grid partition technique, which can guide us to determine a suitable grid partition such that a specified estimation error requirement is satisfied.
- We demonstrate through extensive theoretical and simulation studies that neglecting probabilistic behavior of a region failure may significantly over-estimate or under-estimate its impact on network vulnerability.

The rest of this paper is outlined as follows. Section II introduces the general probabilistic region failure model and the problem formulation of expected flow capacity degradation. In Section III, we develop a grid partition scheme to estimate the average performance degradation caused by a random region failure, and also provide the theoretical analysis on the estimation error from using such grid partition. Section IV presents the numerical results to validate the new region failure model and the grid partition scheme. Finally we conclude this paper in Section V.

II. MODEL AND PROBLEM FORMULATION

In this section, we first define a general probabilistic region failure model, then formulate the expected flow capacity degradation from such a failure as a network zone partition problem.

A. Probabilistic Region Failure Model

It is notable that one common feature of real-world attacks (like the physical bomb explosion, E-bomb or EMP attack) is that the power of such an attack gradually attenuates from its center area to outer area. Due to this common feature, the region failures caused by such attacks always share two common behaviors, i.e., a network component near attack center will fail with high probability (may not always probability 1),
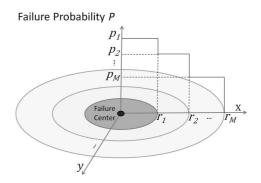

Fig. 1.   Probabilistic Region Failure Model

and such failure probability tends to monotonously decrease as it is farther away from the attack center.

To emulate these common failure behaviors, we introduce here a general probabilistic region failure model.

Definition 1: (**Probabilistic Region Failure Model**) consists of a set of M consecutive annulus, defined by M concentric circles with radius r_i, $i = 1, \ldots, M$, as illustrated in Fig. 1. A network component (like a network node) falling within i-th annulus will fail with probability p_i, where annulus are sequentially numbered from the failure center. To mimic the above behaviors, the following properties hold for p_i:

- The probability p_i is monotonously decreasing, i,e, $p_i \geq p_{i+1}$, $i = 1, \ldots, M-1$.
- The region failure is only confined within the circle area of radius r_M, beyond which the failure probability is regarded as 0.

It is noted our probabilistic region failure (PRF) model is different from the previous "deterministic" failure models in the sense that: 1) it is more general as it covers the former single circular model in [16], [18] as a special case ; 2) it is more realistic as it reflects the monotonously decreasing trend of failure probability for real region failures; 3) it is more flexible and can be configured with different parameter settings to adapt to various realistic scenarios.

Without loss of generality, in the following we focus on the simple two-annulus PRF model with $M = 2$, $p_1 = 1$ and $p_2 = p$ to simply the presentation [1].

B. Problem Formulation

Based on the above PRF model, we will assess the vulnerability of a wireless mesh network under single random region failure. In this paper, we choose to explore the impact of region failure upon some specified key flows (like some mission critical flows), and take the expected flow capacity degradation as the network vulnerability metric [2]. Here, the expected flow capacity degradation is measured over all concerned flows after region failure happens but before initiating the network

---

[1]For a small area around the region failure center, the failure probability there can be high enough to be approximated as 1.

[2]Some other metrics can also be adopted for network vulnerability evaluation, like the vertex based degree centrality [24], the operational O-D pairs or paths, the minimum shortest paths [25]–[27], the critical vertex/edge [28]–[30] and pairwise connectivity [31].

$$w_1=w_2=w_3=C_f \qquad w_4=w_5=w_6=(1-(1-p)^2)\cdot C_f$$
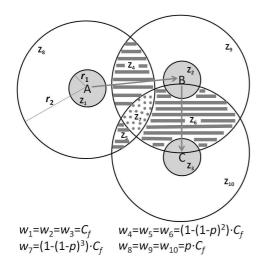$$w_7=(1-(1-p)^3)\cdot C_f \qquad w_8=w_9=w_{10}=p\cdot C_f$$

Fig. 2.   RFL zones $\{Z_i\}$ and their impacts $\{w_i\}$ of a flow

recovery mechanism, so it indicates the possible worst case performance degradation after a region failure. This problem can be defined as follows.

Expected Capacity Degradation Problem: *For a given network and the routing/capacity information of some specified flows in it, calculate the expected capacity degradation of these flows under a random region failure.*

To solve the Expected Capacity Degradation (ECD) problem, one straightforward approach is to first apply the PRF model to partition the overall network area into some disjoint and uniform region failure location (RFL) zones.

Definition 2: (**RFL Zone**) A RFL zone is a network sub-area that any PRF with center falling within it will always induce the same impact (i.e., the same flow capacity degradation) to all the concerned flows.

For a simple scenario of having only one flow f with capacity C_f and 3 nodes, such RFL zone partition is illustrated in Fig. 2, where the network region is divided into different RFL zones $\{Z_i\}$ with impacts $\{w_i\}$, $i=1,...,10$.

Based on the area of each RFL zone and its impact on flow capacity degradation, we can easily evaluate the overall ECD of all concerned flows under a random region failure. For a network with coverage area Z, suppose we have already divided network region into different RFL zones $\{Z_t\}$ with different areas $\{|Z_t|\}$ and impacts $\{w_t\}$, then the overall ECD w can be determined as

$$w = \sum_{Z_t} \frac{|Z_t|}{Z} \cdot w_t \qquad (1)$$

Here $|Z_t|/Z$ is just the probability that the PRF's center falls within the RFL zone Z_t.

To apply (1) for the evaluation of ECD, we need to find out all the RFL zones. Such RFL zones depend on many factors, like the node topology distribution (e.g., distance among nodes, number of nodes), flow distribution (routing path for each concerned flow, number of nodes per flow), and also parameter settings of the PRF model (M and r_i, $i=1,\ldots,M$). Suppose the number of nodes of all concerned flows is N, then we can see that total number of RFL zones

can be as high as $O((M+1)^N)$ in the worst case. Also, finding all these RFL zones and calculating their area involve a lot of very complicated geometric operations. In the next section we present an efficient scheme for the estimation of w.

III. ESTIMATION OF ECD

In this section, we first introduce a grid partition-based scheme for the estimation of ECD, then provide a theoretical analysis on the estimation error from using such grid partition technique.

A. Grid Partition-based Estimation for ECD

Without loss of generality, we assume that the network coverage area is an $b \times b$ square. We apply a grid to evenly divide the $b \times b$ square into $c \times c$ small cells $\{S_j, j = 1, ..., c^2\}$ with side length $a = b/c$ each, as illustrated in Fig. 3. Based on this grid partition, one simple way to estimate the ECD of some concerned flows is to regard each cell here as a "RFL" zone and take the impact of its center point as the impact of this cell. In this way, we can get an estimation of ECD based on the (1).

Suppose that the set of concerned flows are $\{f_k, k = 1, ..., K\}$, and let (x_j^*, y_j^*) be the central point of j_{th} cell S_j, and let $w_{f_k}(x, y)$ be the induced impact on flow f_k when PRF center is at point (x, y). Then the grid partition-based scheme for obtaining an estimation $\hat{w}$ of ECD can be summarized as the following Algorithm 1.

Algorithm 1 ECD Estimation:
Input: The network grid partition information, flow distribution and failure model parameters;
Output: ECD estimation $\hat{w}$;

1. $\hat{w} \Leftarrow 0$;
2. **for** $k = 1$ to K **do**
3.   **for** $j = 1$ to c^2 **do**
4.   calculate $w_{f_k}(x_j^*, y_j^*)$;
5. $\hat{w} = \hat{w} + (a^2/b^2) \cdot w_{f_k}(x_j^*, y_j^*)$;
6.   **end for**
7. **end for**
8. **return** $\hat{w}$;

In the Algorithm 1, we take the central point (x_j^*, y_j^*) of cell S_j as the sampling point and simply use its impact $w_{f_k}(x_j^*, y_j^*)$ as an approximation of the impact of all other points in S_j. Since each cell here may not be a RFL zone, such approximation will cause an estimation error between $\hat{w}$ and w. For a flow with two nodes and capacity C_f, a partition cell S_j that intersects with three RFL zones there is illustrated in the Fig. 3. Notice that the three RFL zones intersecting with S_j have distinct impacts of 0, $p \cdot C_f$ and $(1 - (1 - p)^2) \cdot C_f$, respectively. Thus, talking the impact $p \cdot C_f$ of the center (x_j^*, y_j^*) of S_j as an approximation of the impacts of all other points (can be 0 or $(1 - (1 - p)^2) \cdot C_f$ here) will induce estimation error in the calculation of ECD w.
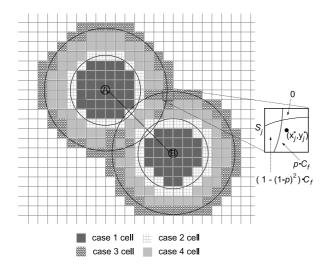
Fig. 3. Illustration of network grid partition and ECD estimation error for a flow with only two nodes A and B. The cells of cases 2 and 3 will introduce ECD estimation error while the cells of cases 1 and 4 will not.

In the next subsection, we provide a theoretical model on the possible estimation error that the Algorithm 1 may introduce in the estimation of w. Such a model can help us to determine a suitable grid partition (i.e., a suitable cell size a) such that a specified estimation error requirement is satisfied.

B. ECD Estimation Error Modeling

Based on the grid partition introduced above, the ECD w and its estimation $\hat{w}$ for the set of concerned flows $\{f_k, k = 1, ..., K\}$ can be expressed as

$$w = \frac{1}{b^2} \cdot \sum_{k=1}^{K} \sum_{j=1}^{c^2} \iint_{(x,y) \in S_j} w_{f_k}(x,y) \mathrm{d}x\mathrm{d}y \quad (2)$$

$$\hat{w} = \frac{1}{b^2} \cdot \sum_{k=1}^{K} \sum_{j=1}^{c^2} \iint_{(x,y) \in S_j} w_{f_k}(x_j^*, y_j^*) \mathrm{d}x\mathrm{d}y \quad (3)$$

If we use Δ to denote the estimation error of w, then we have

$$\Delta = |w - \hat{w}|$$
$$\leq \sum_{k=1}^{K} \left| \frac{1}{b^2} \sum_{j=1}^{c^2} \iint_{(x,y) \in S_j} \left(w_{f_k}(x_j^*, y_j^*) - w_{f_k}(x,y) \right) \mathrm{d}x\mathrm{d}y \right| \quad (4)$$

The (4) indicates that the overall estimation error Δ is no more than the sum of estimation error for the ECD of each flow. If we use Δ_{f_k} to denote the estimation error for the ECD of flow f_k, then we have

$$\Delta_{f_k} = \left| \frac{1}{b^2} \sum_{j=1}^{c^2} \iint_{(x,y) \in S_j} \left(w_{f_k}(x_j^*, y_j^*) - w_{f_k}(x,y) \right) \mathrm{d}x\mathrm{d}y \right| \quad (5)$$

$$\leq \sum_{j=1}^{c^2} \left| \frac{1}{b^2} \iint_{(x,y) \in S_j} \left(w_{f_k}(x_j^*, y_j^*) - w_{f_k}(x,y) \right) \mathrm{d}x\mathrm{d}y \right| \quad (6)$$

The (6) says that the estimation error Δ_{f_k} for flow f_k is upper bounded by the sum of corresponding estimation error introduced in each cell. If we use $\Delta_{f_k}^{S_j}$ to denote the maximum difference between the average impact (on f_k) of any two points in S_j, i.e.,

$$\Delta_{f_k}^{S_j} = \max_{(x,y) \in S_j} \{w_{f_k}(x,y)\} - \min_{(x,y) \in S_j} \{w_{f_k}(x,y)\} \quad (7)$$

then we have

$$\left| \frac{1}{b^2} \iint_{(x,y) \in S_j} \left(w_{f_k}(x_j^*, y_j^*) - w_{f_k}(x,y) \right) \mathrm{d}x\mathrm{d}y \right|$$
$$\leq \frac{1}{b^2} \iint_{(x,y) \in S_j} \left| w_{f_k}(x_j^*, y_j^*) - w_{f_k}(x,y) \right| \mathrm{d}x\mathrm{d}y$$
$$\leq \frac{1}{b^2} \iint_{(x,y) \in S_j} \Delta_{f_k}^{S_j} \mathrm{d}x\mathrm{d}y$$
$$= \frac{1}{c^2} \Delta_{f_k}^{S_j} \quad (8)$$

Combining (4), (5), (6) and (8), we have

$$\Delta \leq \sum_{k=1}^{K} \Delta_{f_k} \leq \sum_{k=1}^{K} \sum_{j=1}^{c^2} \frac{1}{c^2} \Delta_{f_k}^{S_j} \quad (9)$$

The (9) shows that we can control the overall estimation error Δ by properly selecting the number of cells c (or equivalently the size $a = b/c$ of each cell) in the grid-partition based ECD estimation. Let C_k denote the capacity of concerned flow f_k, $k = 1, ..., K$, then we can define the following ECD estimation error bounding problem.

ECD Estimation Error Bounding Problem: *For an error requirement $\epsilon > 0$, to determine a low bound c_ϵ on the number of cells c, such that when $c > c_\epsilon$ we can always guarantee that*

$$\Delta \leq \sum_{k=1}^{K} \sum_{j=1}^{c^2} \frac{1}{c^2} \Delta_{f_k}^{S_j} \leq \epsilon \cdot \sum_{k=1}^{K} C_k \quad (10)$$

The (10) indicates that to determine the lower bound c_ϵ for a given ϵ, we need to identify each cell that has non-zero term $\Delta_{f_k}^{S_j}$ (i.e., the cell that introduces estimation error) and also to determine the total number of such cells, as discussed in the following subsections.

C. Identification of Cells with Estimation Error

Based on the simple two-annulus PRF model introduced in Section II-A, we can easily see that the area around a network node can also be divided into two same annulus (as shown in Fig. 3), where a PRF with center falling within the inner annulus (resp. the outer annulus) will cause the node to fail with probability 1 (resp. probability p). Thus, for a given flow f_k, whether a cell will introduce ECD estimation error for this flow depends on how the cell intersects with the boundaries of the outer annulus and inner annulus of all the nodes of this flow (hereafter, we call these annulus as the annulus of this flow). To characterize such intersection between a cell S and the annulus of flow f_k, we define a four-tuple (m_k, n_k, h_k, g_k), which indicates that the cell partially intersects with the boundaries of m_k outer annulus and h_k

inner annulus of flow f_k, but it completely falls within other n_k outer annulus and g_k inner annulus of the flow.

Based on the four-tuple (m_k, n_k, h_k, g_k) for flow f_k and a cell S, the $\Delta_{f_k}^S$ defined by (7), i.e., the maximum difference between the average impact (on f_k) of any two points in S, can be determined as

$$
\Delta_{f_k}^S = \begin{cases} 0 & \text{case 1: if } g_k \geq 1, \\ C_k \cdot q^{n_k} & \\ & \text{case 2: if } g_k = 0, h_k \geq 1, \\ C_k \cdot q^{n_k} \cdot \left(1 - q^{m_k}\right) & \\ & \text{case 3: if } g_k = 0, h_k = 0, m_k \geq 1, \\ 0 & \text{case 4: if } g_k = 0, h_k = 0, m_k = 0. \end{cases} \tag{11}
$$

where $q = 1 - p$ is the non-failure probability of a node falling within the outer annulus defined by the simple two-annulus PRF model in Section II.A. The (11) indicates clearly that only the cells of the cases 2 and 3 will introduce ECD estimation error for the flow f_k, as illustrated in the Fig. 3.

Let $u_k(\lambda)$ denote the total number of cells of the case 2 with $n_k = \lambda$, and let $v_k(\beta, \gamma)$ denote the total number of cells of the case 3 with $m_k = \beta$ and $n_k = \gamma$, then the overall ECD estimation error for the flow f_k is given by

$$
\begin{aligned}
\sum_{j=1}^{c^2} & \frac{1}{c^2} \Delta_{f_k}^{S_j} \\
&= \frac{C_k}{c^2} \cdot \left(\sum_{\lambda \geq 1} u_k(\lambda) q^\lambda + \sum_{\beta \geq 1, \gamma \geq 0} v_k(\beta, \gamma) \left(1 - q^\beta\right) q^\gamma \right)
\end{aligned} \tag{12}
$$

D. Counting the Cells with Estimation Error

The (10) and (12) indicate that to solve the overall estimation error bounding problem, we need to determine the values of $u_k(\lambda)$ and $v_k(\beta, \gamma)$ for each flow f_k with $\lambda \geq 1$, $\beta \geq 1$ and $\gamma \geq 0$. However, determining the exact value of $u_k(\lambda)$ and $v_k(\beta, \gamma)$ for each flow f_k is still a very difficult task, which involves the complicated geometric operation to identify the relationship (intersecting or containing) between cells and annulus boundaries of a flow. We instead provide here a tractable upper bound to efficiently approximate the ECD estimation error in (12).

Notice from the Fig. 3 that the effect of a PRF upon a network node is defined by the two annulus around the node, and our basic idea here is to first derive a general "node-level estimation error (NEE)" for each node of flow f_k based on the intersection between its two annulus and cells around the node, then apply the NEE of each node to get a general bound on the ECD estimation error of this flow.

To get a general NEE for each node, we need to identify all the cells around a node that will "contribute" to the ECD estimation error. For this purpose, we consider a tagged node A and one its neighbor node B that is d_{max} away, as illustrated in Fig. 4. Here the d_{max} is defined as the maximum distance between any two neighbor nodes of any flow, which is controlled by the maximum communication range (or power) of the network. We use $\mathbb{C}_{in}^A$ and $\mathbb{C}_{out}^A$, $\mathbb{C}_{in}^B$ and $\mathbb{C}_{out}^B$ to denote
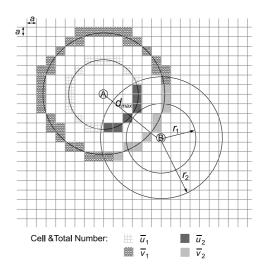

Fig. 4. Illustration for the cell counting, where the distance between the nodes A and B is fixed as d_{max}, and the network is partitioned with cells of size a each.

the inner annulus and outer annulus of A and B, respectively. Then the cells that may introduce ECD estimation error to the node A can be defined by the following variables:

- $\bar{v}_1$: the number of cells partially intersecting with the boundary of $\mathbb{C}_{out}^A$ but not completely falling within $\mathbb{C}_{in}^B \cup \mathbb{C}_{out}^B$.
- $\bar{v}_2$: the number of cells partially intersecting with the boundary of $\mathbb{C}_{out}^A$ and completely falling within $\mathbb{C}_{in}^B \cup \mathbb{C}_{out}^B$.
- $\bar{u}_1$: the number of cells partially intersecting with the boundary of $\mathbb{C}_{in}^A$ but not completely falling within the $\mathbb{C}_{in}^B \cup \mathbb{C}_{out}^B$.
- $\bar{u}_2$: if $\bar{u}_1 > 0$, $\bar{u}_2$ is defined as the total number of cells that partially intersect with the boundary of $\mathbb{C}_{in}^A$ and completely fall within the $\mathbb{C}_{in}^B \cup \mathbb{C}_{out}^B$. In the case $\bar{u}_1 = 0$, $\bar{u}_2$ is the number of cells that partially intersect with the boundary of $\mathbb{C}_{in}^A$ and not completely fall within the $\mathbb{C}_{in}^B$.

For the example shown in Fig. 4, we can easily prove that the $\bar{u}_1, \bar{u}_2, \bar{v}_1$ and $\bar{v}_2$ there are given by the formulas in Table I and II.

Remark 1: The values of $\bar{u}_1, \bar{u}_2, \bar{v}_1$ and $\bar{v}_2$ in Tables I and II are only determined by the network parameters d_{max}, r_1 and r_2 and thus independent of flows.

Remark 2: For the tagged node A and its neighbor node B in Fig. 4, the boundaries of their outer annulus are not intersecting with the network boundary. Thus, the results in Tables I and II represent the maximum values of $\bar{u}_1, \bar{u}_2, \bar{v}_1$ and $\bar{v}_2$.

Based on the $\bar{u}_1, \bar{u}_2, \bar{v}_1$ and $\bar{v}_2$ in the Tables I and II, we can define NEE_k (i.e., the NEE for each node of flow f_k) as

$$
NEE_k = \frac{C_k}{c^2} \cdot \left(\bar{u}_1 q + \bar{u}_2 q^2 + \bar{v}_1 p + \bar{v}_2 pq \right) \tag{13}
$$

We now show that the NEE_k can be used to establish an upper bound for the overall ECD estimation error (12)

TABLE I
$\bar{u}_1$ AND $\bar{u}_2$

d_{max}	$\bar{u}_1$	$\bar{u}_2$
$d_{max} \leq r_2 - r_1 \ \& \ r_2 \leq 3r_1$ or $d_{max} \leq 2r_1 \ \& \ r_2 > 3r_1$	0	$4\lceil \frac{2r_1}{a} \rceil - 4\lceil \frac{2r_1}{a} \rceil \frac{1}{\pi} \cos^{-1}\frac{d_{max}}{2r_1}$
$2r_1 < d_{max} \leq r_2 - r_1 \ \& \ r_2 > 3r_1$	0	$4\lceil \frac{2r_1}{a} \rceil$
$r_2 - r_1 < d_{max} \leq r_2 + r_1$	$4\lceil \frac{2r_1}{a} \rceil - \bar{u}_2$	$4\lceil \frac{2r_1}{a} \rceil \frac{1}{\pi} \cos^{-1}\frac{d_{max}{}^2 + r_1{}^2 - r_2{}^2}{2d_{max}r_1}$
$d_{max} > r_2 + r_1$	$4\lceil \frac{2r_1}{a} \rceil$	0

TABLE II
$\bar{v}_1$ AND $\bar{v}_2$

d_{max}	$\bar{v}_1$	$\bar{v}_2$
$d_{max} \leq 2r_2$	$4\lceil \frac{2r_2}{a} \rceil - \bar{v}_2$	$4\lceil \frac{2r_2}{a} \rceil \frac{1}{\pi} \arccos \frac{d_{max}}{2r_2}$
$d_{max} > 2r_2$	$4\lceil \frac{2r_2}{a} \rceil$	0

of the flow f_k, as summarized in the following lemma (See Section VI for the proof).

Lemma 1: Given the PRF model parameters r_1 and r_2, cell side length a, then for any flow f_k, $1 \leq k \leq K$, we have

$$\frac{C_k}{c^2} \cdot \left(\sum_{\lambda \geq 1} u_k(\lambda)q^\lambda + \sum_{\beta \geq 1, \gamma \geq 0} v_k(\beta, \gamma)(1 - q^\beta)q^\gamma \right)$$
$$\leq N_k \cdot NEE_k \tag{14}$$

E. A Lower Bound for Estimation Error Guarantee

By combining the (10), (12) and (14), we can easily prove the following theorem regarding a lower bound c_ϵ of c for a specified error requirement ϵ.

Theorem 1: For a specified error requirement $\epsilon > 0$, we can determine a lower bound c_ϵ for c as follows such that when $c \geq c_\epsilon$, the (10) always holds.

1) when $d_{max} \leq r_2 - r_1 \ \& \ r_2 \leq 3r_1$, or $d_{max} \leq 2r_1 \ \& \ r_2 > 3r_1$,

$$c_\epsilon = \frac{8}{\epsilon \pi b \sum_{k=1}^{K} C_k}$$
$$\times \sum_{k=1}^{K} N_k C_k \Big(r_1(\pi - \arccos \frac{d_{max}}{2r_1})(1 - p)^2$$
$$+ \ r_2(\pi - p \arccos \frac{d_{max}}{2r_2}) \cdot p \Big) \tag{15}$$

2) when $2r_1 < d_{max} \leq r_2 - r_1 \ \& \ r_2 > 3r_1$,

$$c_\epsilon = \frac{8}{\epsilon \pi b \sum_{k=1}^{K} C_k} \sum_{k=1}^{K} N_k C_k \Big(r_1 \pi (1 - p)^2$$
$$+ r_2(\pi - p \arccos \frac{d_{max}}{2r_2}) \cdot p \Big) \tag{16}$$

3) when $r_2 - r_1 < d_{max} \leq r_2 + r_1$,

$$c_\epsilon = \frac{8}{\epsilon \pi b \sum_{k=1}^{K} C_k}$$
$$\times \sum_{k=1}^{K} N_k C_k \Big(r_1(\pi - \arccos \frac{d_{max}^2 + r_1^2 - r_2^2}{2d_{max}r_1})(1 - p)$$
$$+ \ r_1 \arccos \frac{d_{max}^2 + r_1^2 - r_2^2}{2d_{max}r_1}(1 - p)^2$$
$$+ \ r_2(\pi - p \arccos \frac{d_{max}}{2r_2}) \cdot p \Big) \tag{17}$$

4) when $r_2 + r_1 < d_{max} \leq 2r_2$,

$$c_\epsilon = \frac{8}{\epsilon \pi b \sum_{k=1}^{K} C_k} \sum_{k=1}^{K} N_k C_k \Big(r_1 \pi (1 - p)$$
$$+ r_2(\pi - p \arccos \frac{d_{max}}{2r_2}) \cdot p \Big) \tag{18}$$

5) when $d_{max} > 2r_2$,

$$c_\epsilon = \frac{8}{\epsilon b \sum_{k=1}^{K} C_k} \sum_{k=1}^{K} N_k C_k \Big(r_1(1 - p) + r_2 p \Big) \tag{19}$$

IV. NUMERICAL RESULTS

In this section, we first verify the efficiency of the ECD estimation scheme through simulation, then apply it to assess the network vulnerability under the new PRF model.
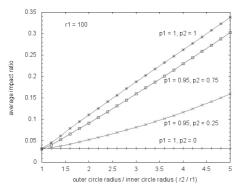
A. Simulation Setting

We developed a simulator in C++ to simulate the impact of a random PRF upon on some specified flows. Similar to the settings used in [16], we consider a random network with 32 nodes, in which the coordinates (x, y) of each node are uniformly generated in a $2000 \times 2000 \ m^2$ field. We randomly generate eight flows, where the number of nodes per flow is drawn randomly in $[3, 5]$, each link distance is drawn randomly in $[100, 400] \ m$, and the flow capacity is drawn randomly in $[3, 10]$ Mbps. The final network graph for simulation is shown in Fig. 8a, in which the maximum distance between any two neighbor nodes of any flow is determined as $d_{max} = 360.555$. The metric adopted for performance evaluation is the average impact ratio (AIR), defined as
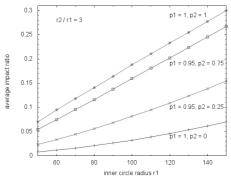
$$AIR = \frac{w}{\sum_{k=1}^{K} C_k} \tag{20}$$

The simulated AIR was calculated as the average value of ten batches of simulation results, where each batch consists of one million random and independent simulations.

B. PRF Model and "Deterministic" Failure Models

To illustrate how the general PRF model is different from the "Deterministic" failure models, we first conducted a simulation under the general parameter setting for (p_1, p_2). The Fig. 5 illustrates the variations of AIR with the parameters (r_1, r_2, p_1, p_2), where the settings $(p_1 = 1, p_2 = 1)$ and $(p_1 = 1, p_2 = 0)$ correspond to the "deterministic" model scenarios.

(a) Average Impact Ratio vs. r_2/r_1

(b) Average Impact Ratio vs. r_1

Fig. 5. PRF Model and "Deterministic" Failure Models.

The results here indicate clearly that the "deterministic" models, although simple and easy to use, may result in a significant overestimation or underestimation of network vulnerability. For example, when we set $r_2/r_1 = 3.6$ in Fig. 5a, we get an average impact ratio of 0.102 with the setting of $(p_1 = 0.95, p_2 = 0.25)$, while this ratio decreases to 0.032 with the setting of $(p_1 = 1, p_2 = 0)$. Regarding the results of fixed r_2/r_1 in Fig. 5b, we can see that when $r_1 = 80$, the average impact ratio is estimated as 0.116 for the case $(p_1 = 0.95, p_2 = 0.75)$, and this estimated ratio increases to 0.141 when both p_1 and p_2 are regarded as 1 there. It is also interesting to note that as r_1 (or r_2/r_1) increases (and thus failure region becomes bigger), the estimation gap between the probabilistic model and the corresponding "deterministic" ones tends to increase sharply, and such gaps can be very significant if the probabilistic feature of region failure is not properly "rounded-off".

C. ECD Estimation Scheme Validation

To verify the the ECD estimation scheme, further simulation was conducted under the simple PRF model of $(p_1 = 1, p_2 = p)$. The parameters used in the simulation are summarized in Table III, where each case of parameter setting is corresponding to one individual case discussed in the Theorem 1. We verified the ECD estimation scheme under two error requirements of $\epsilon = 0.01$ and $\epsilon = 0.005$. The corresponding simulation results and estimation results from our scheme are summarized in the Table IV.

The Table IV indicates clearly that when we set $c \geq c_\epsilon$,

TABLE III
FAILURE MODEL PARAMETER SETTINGS

	p	r_1	r_2
case 1	0.50	50	100
case 2	0.35	80	200
case 3	0.25	100	500
case 4	0.75	180	200
case 5	0.15	200	600
case 6	0.10	200	700

TABLE IV
COMPARISON BETWEEN SIMULATION AND ESTIMATION RESULTS FOR MODEL VALIDATION, $C = \sum_{k=1}^{8} C_k$

		w/C	$\hat{w}/C$	Δ/C	c_ϵ
case 1	$\epsilon = 0.01$	0.0201332	0.0200634	6.98e-005	126
	$\epsilon = 0.005$	0.0201248	0.0201419	1.70e-005	252
case 2	$\epsilon = 0.01$	0.05511	0.0550707	3.93e-005	199
	$\epsilon = 0.005$	0.0551315	0.0551305	1.03e-006	398
case 3	$\epsilon = 0.01$	0.160276	0.160349	7.28e-005	284
	$\epsilon = 0.005$	0.160279	0.160315	3.62e-005	569
case 4	$\epsilon = 0.01$	0.106664	0.106649	1.47e-005	295
	$\epsilon = 0.005$	0.106683	0.106636	4.70e-005	590
case 5	$\epsilon = 0.01$	0.193783	0.193646	1.36e-004	350
	$\epsilon = 0.005$	0.193819	0.19378	3.96e-005	701
case 6	$\epsilon = 0.01$	0.189801	0.18987	6.90e-005	346
	$\epsilon = 0.005$	0.189838	0.189847	9.57e-006	693

our scheme could provide an efficient estimation for the AIR, and the induced overall estimation error is always less than the specified ϵ. It is also notable that for each test case here, the actual error between the simulation and estimation results is several orders smaller than the specified ϵ. This very small overall estimation error (and thus a very safe c_ϵ) are due to the following facts. The first factor is that the maximum possible estimation error (rather than the real estimation error) of each cell is adopted in the evaluation of the overall ECD estimation error (Eq. 12). The second factor lies in that the estimation of the number of error-inducing cells in (13), in which only the maximum values for $\bar{u}_1$ and $\bar{v}_1$ are considered, while the errors of other cells are approximated through $\bar{u}_2$ and $\bar{v}_2$. The last factor is that the distance between any two neighbor nodes is always regarded as d_{max} in the Theorem 1, which helps us to derive an unified and closed form formula for c_ϵ but leads to an overestimation for the parameter.

The above results indicate that our ECD estimation scheme and the related theoretical framework for estimation error bounding, although may lead to a "conservative" estimation for the overall ECD, are simple and efficient. To apply such scheme, we just need to divide the network area into $c \times c$ cells and simply use the central point of each cell to calculate the ECD metric, which avoids the complicated geometric operations for the identification and area evaluation of all RFL zones. As long as the cell size a is small enough (or equivalently the number of cells c is big enough such that $c \geq c_\epsilon$), our scheme can always result in a very efficient estimation for the ECD with an error upper bounded by ϵ.

Hereafter, the numerical results in performance evaluation are obtained based on our ECD estimation scheme, where the simple PRF model of $(p_1 = 1, p_2 = p)$ and an error requirement of $\epsilon = 0.005$ are assumed.
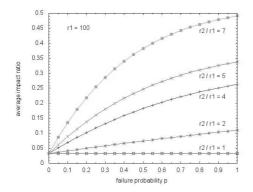
Fig. 6.   Average Impact Ratio vs. Failure Probability p
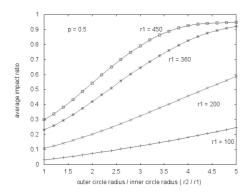

Fig. 7.   Average Impact Ratio vs. r_2/r_1.

D. Average Impact Ratio vs. Failure Model Parameters

The Fig. 6 shows the relationship between the AIR and the failure probability p under different settings of r_2/r_1, where the setting $r_2/r_1 = 1$ corresponds to a "deterministic" model. We can see from the Fig. 6 that with $r_1 = 100$, a non-negligible AIR difference between $r_2/r_1 > 1$ (r_2/r_1 =2,4,5,7) and $r_2/r_1 = 1$ can be observed even for a very small value of the failure probability p. For example, when $p = 0.2$, the AIR of the scenario $r_2/r_1 = 2$ is 0.050, which is nearly 1.56 times as that of the scenario $r_2/r_1 = 1$ (0.032 there); for the case that $p = 0.35$, the AIR of the first scenario (0.062) is nearly 1.94 times as that of the later case (0.032). The Fig. 6 also shows clearly that as r_2 or p increase, the AIR difference between $r_2/r_1 > 1$ and $r_2/r_1 = 1$ increases sharply. This results indicates that even for a very small failure probability p, the probabilistic outer annulus part of a PRF may significantly affect the overall network capacity.

When failure probability is set as $p = 0.5$, the relationship between AIR and r_2/r_1 is illustrated in the Fig. 7. We can see from the figure that in general, as r_1 increases, the AIR becomes more sensitive to the variation of the ratio r_2/r_1. For example, when r_2/r_1 varies from 1.6 to 3.6, the AIR for the scenario of $r_1 = 100$ varies from 0.056 to 0.159 and the AIR for the scenario of $r_1 = 200$ varies from 0.162 to 0.404, respectively. The results here also show clearly that for the case $r_1 = 450$, the AIR is not sensitive to the variation of r_2/r_1 anymore as it increases beyond the point $r_2/r_1 = 4.4$. This is because that when r_1 and r_2 are large enough, the PRF starts to cover the whole network area and thus all the flows. A

(a) Network topology   (b) Vulnerable zone distribution
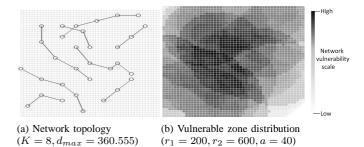($K = 8, d_{max} = 360.555$)   ($r_1 = 200, r_2 = 600, a = 40$)

Fig. 8.   Network topology and vulnerable network zone distribution estimated by our scheme.

more careful observation of the Fig. 7 indicates that even with a PRF of $r_1 = 360$ (roughly same as the $d_{max} = 360.555$) and $r_2/r_1 = 2.4$, we may achieve an over 50% reduction (i.e., $AIR > 0.5$) to the overall capacity of the concerned flows.

E. Vulnerable Network Zone Identification

In our grid partition-based ECD estimation scheme, we divide the whole network area equally into $c \times c$ cells, then take the central point of each cell as the sampling point and use its impact to approximate the impact of the cell. Thus, one attractive application of the estimation scheme is that it helps us to identify the geographical distribution and size of the vulnerable network zones.

For the network adopted in our study (Fig. 8a) and the setting of ($r_1 = 200, r_2 = 600, a = 40$), the vulnerable network zone distribution estimated by our scheme is illustrated in Fig. 8b. Based on such vulnerable network zone distribution, one can also easily identify the most vulnerable network zone(s), i.e., the zones in which each cell there has the biggest impact to the network flow capacity. Such vulnerable network zone distribution and the most vulnerable network zone information will be helpful for network designers to initiate proper network protection strategy against region failures.

V. CONCLUSION

In this paper, we proposed a more realistic probabilistic region failure (PRF) model to capture some main features of geographically correlated region failures, and then developed a framework to apply the PRF model for the vulnerability assessment of wireless mesh networks. Our results indicate that neglecting some key properties of real region failures can result in a significant overestimation or underestimation of network vulnerability, which may mislead network designers in initiating proper and cost-efficient network protection against such failures. It is expected that our work in this paper will contribute to the future network design and planning against possible region failures.

Some possible extensions of this work are:
- Routing issue: Notice that our framework in this paper can be applied to evaluate a network with a given routing strategy. How to apply this work and the corresponding results (like the vulnerable network zone distribution

information) to find efficient and region failure-tolerant routing algorithm to alleviate the impacts of region failure can be an interesting work.

- Recovery issue: We only considered the PRF impact before network recovery (like topology reconfigure and flow rerouting), so it only indicates the worst case network performance degradation. How to extend this work to estimate the network performance degradation (like the flow capacity degradation) after network recovery deserves further study.

- Vulnerability under other metrics: To have a more deeper understanding of network vulnerability under PRF, another future work is to extend the framework established in this paper to further evaluate the network performance degradation under other metrics, like the pairwise connectivity [31], critical vertex/edge [28]–[30], etc.

VI. APPENDIX

Based on the (12) and (13) we know that to prove the (14), we just need to show that for any f_k the following condition holds

$$\sum_{\lambda \geq 1} u_k(\lambda)q^\lambda + \sum_{\beta \geq 1, \gamma \geq 0} v_k(\beta, \gamma)\big(1 - q^\beta\big)q^\gamma$$
$$\leq N_k\big(\bar{u}_1 q + \bar{u}_2 q^2 + \bar{v}_1 p + \bar{v}_2 pq\big) \qquad (21)$$

From the discussion in Section III-C we know that only the cells of cases 2 and 3 in (11) will introduce the ECD estimation error. We first consider the first term regarding the case 2 cells in the left side of (21), i.e., the term $\sum_{\lambda \geq 1} u_k(\lambda)q^\lambda$. Since the d_{max} is the maximum distance between any two neighbor nodes of any flow, it is trivial to see that $u_k(1) \leq N_k \cdot \bar{u}_1$. Based on the definitions of $\bar{u}_1$ and $\bar{u}_2$, and also notice that q^λ monotonically decreases as λ increases, we have

$$\sum_{\lambda \geq 1} u_k(\lambda)q^\lambda \leq N_k\big(\bar{u}_1 q + \bar{u}_2 q^2\big) \qquad (22)$$

Similarly, for the cells belonging to the case 3 in (11), we have the following inequalities for any f_k

$$\sum_{\beta \geq 1} \beta \cdot v_k(\beta, 0) \leq N_k \cdot \bar{v}_1 \qquad (23)$$

and

$$\sum_{\beta \geq 1, \gamma \geq 1} \beta \cdot v_k(\beta, \gamma) \leq N_k \cdot \bar{v}_2 \qquad (24)$$

Now we consider the second term in the left side of (21), i.e., $\sum_{\beta \geq 1, \gamma \geq 0} v_k(\beta, \gamma)\big(1 - q^\beta\big)q^\gamma$, where the component $(1 - q^\beta)q^\gamma$ increases with β but decreases with γ. Since some cells of the case 3 are associated with a big value of β but a small value of γ, we can not directly derive a similar inequality like the (22) for the case 3 cells. For a case 3 cell S_j counted as $v_k(\beta, \gamma)$, its maximum estimation error, i.e., the maximum difference between the average impact (on f_k) of any two

points in it, is given by

$$\Delta_{f_k}^{S_j} = C_k q^\gamma \big(1 - q^\beta\big)$$
$$= C_k q^\gamma \sum_{i=1}^{\beta} (-1)\binom{\beta}{i}(-p)^i$$
$$\leq C_k q^\gamma \cdot p \cdot \beta$$
$$= C_k q^\gamma \big(1 - q\big) \cdot \beta \qquad (25)$$

Based on the (25), we first establish the following results regarding the second term in the left side of (21) under the special case that $\beta \geq 1$ and $\gamma = 0$,

$$\sum_{\beta \geq 1} v_k(\beta, 0)\big(1 - q^\beta\big)$$
$$\leq \sum_{\beta \geq 1} v_k(\beta, 0) \cdot p \cdot \beta \qquad (26)$$
$$= \sum_{\beta \geq 1} \beta \cdot v_k(\beta, 0) \cdot p$$
$$\leq N_k \cdot \bar{v}_1 \cdot p \qquad (27)$$

where inequalities (26) and (27) are due to the (25) and (23), respectively.

We now show that for the general case $\beta \geq 1$, $\gamma \geq 1$, we have

$$\sum_{\beta \geq 1, \gamma \geq 1} v_k(\beta, \gamma)\big(1 - q^\beta\big)q^\gamma$$
$$\leq \sum_{\beta \geq 1, \gamma \geq 1} v_k(\beta, \gamma) \cdot q^\gamma \cdot p \cdot \beta \qquad (28)$$
$$\leq \sum_{\beta \geq 1, \gamma \geq 1} \beta \cdot v_k(\beta, \gamma) \cdot q \cdot p$$
$$\leq N_k \cdot \bar{v}_2 \cdot q \cdot p \qquad (29)$$

where inequalities (28) and (29) are due to the (25) and (24), respectively.

Combining the (27) and (29), the following inequality for the cells of case 3 follows,

$$\sum_{\beta \geq 1, \gamma \geq 0} v_k(\beta, \gamma)\big(1 - q^\beta\big)q^\gamma \leq N_k\big(\bar{v}_1 p + \bar{v}_2 pq\big) \qquad (30)$$

Finally, the (21) comes after the (22) and (30).

REFERENCES

[1] M. Khabbazian, H. Mercier, and V. K. Bhargava, "Severity analysis and countermeasure for the wormhole attack in wireless ad hoc networks," *IEEE Transactions on Wireless Communications*, vol. 8, no. 2, pp. 736–745, 2009.

[2] Y. Zhang, W. Liu, W. Lou, and Y. Fang, "Mask: anonymous on-demand routing in mobile ad hoc networks," *IEEE Transactions on Wireless Communications*, vol. 5, no. 9, pp. 2376–2385, 2006.

[3] X. Du, M. Guizani, Y. Xiao, and H.-H. Chen, "Two tier secure routing protocol for heterogeneous sensor networks," *IEEE Transactions on Wireless Communications*, vol. 6, no. 9, pp. 3395–3401, 2007.

[4] H. Nakayama, S. Kurosawa, A. Jamalipour, Y. Nemoto, and N. Kato, "A dynamic anomaly detection scheme for aodv-based mobile ad hoc networks," *IEEE Transactions on Vehicular Technology*, vol. 58, no. 5, pp. 2471–2481, 2009.

[5] M. Yu and L. K. K, "A trustworthiness-based qos routing protocol for wireless ad hoc networks," *IEEE Transactions on Wireless Communications*, vol. 8, no. 4, pp. 1888–1898, 2009.

[6] S. Stefanakos, "Reliable routing in networks with generalized link failure events," *IEEE/ACM Transactions on Networking*, vol. 16, no. 6, pp. 1331–1339, December 2008.

[7] B. Awerbuch, D. Holmer, C. Nita-Rotaru, and H. Rubens, "An on-demand secure routing protocol resilient to byzantine failures," in *Proc. of ACM Wise*, 2002.

[8] V. Bhandari and N. H. Vaidya, "Reliable broadcast in wireless networks with probabilistic failures," in *INFOCOM*, 2007.

[9] S. Yu and Y. Zhang, "R-sentry: providing continuous sensor services against random node failures," in *37th Annual IEEE/IFIP International Conference on Dependable Systems and Networks*, 2007, pp. 235–244.

[10] S. Nelakuditi, S. Lee, Y. Yu, Z.-L. Zhang, and C.-N. Chuah, "Fast local rerouting for handling transient link failures," *IEEE/ACM Transactions on Networking*, vol. 15, no. 2, pp. 359–372, April 2007.

[11] R. S. Bhatia, M. Kodialam, T. V. Lakshman, and S. Sengupta, "Bandwidth guaranteed routing with fast restoration against link and node failures," *IEEE/ACM Transactions on Networking*, vol. 16, no. 6, pp. 1321–1330, December 2008.

[12] K.-W. Kwong, L. Gao, R. Guerin, and Z.-L. Zhang, "On the feasibility and efficiency of protection routing in ip networks," in *INFOCOM*, 2010.

[13] R. Banner and A. Orda, "Designing low-capacity backup networks for fast restoration," in *INFOCOM*, 2010.

[14] J. S. F. J. et al., "Report of the commission to assess the threat to the united states from electromagnetic pulse (emp) attack, volume 1: executive peport," Apr. 2004.

[15] W. Radasky, "High-altitude electromagnetic pulse (hemp): a threat to our way of life," in *IEEE-USA Today's Engineer*, Sep. 2007.

[16] A. Sen, B. H. Shen, L. Zhou, and B. Hao, "Fault-tolerance in sensor networks: a new evaluation metric," in *INFOCOM*, 2006.

[17] S. Neumayer, G. Zussman, R. Cohen, and E. Modiano, "Assessing the vulnerability of geographically correlated network failures," in *MILCOM*, 2008.

[18] ——, "Assessing the vulnerability of the fiber infrastructure to disasters," in *INFOCOM*, 2009, pp. 1566–1574.

[19] S. Neumayer and E. Modiano, "Network reliability with geographically correlated failures," in *INFOCOM*, 2010.

[20] A. Sen, S. Banerjee, P. Ghosh, and S. Shirazipourazad, "Impact of region-based faults on the connectivity of wireless networks," in *Proceedings of the 47th annual Allerton conference on Communication, control, and computing, Monticello, Illinois, USA*, 2009, pp. 1430–1437.

[21] A. Sen, S. Murthy, and S. Banerjee, "Region-based connectivity: a new paradigm for design of fault-tolerant networks," in *Proceedings of the 15th international conference on High Performance Switching and Routing, Paris, France*, 2009, pp. 94–100.

[22] Y. Xu and W. Wang, "Characterizing the spread of correlated failures in large wireless networks," in *INFOCOM*, 2010.

[23] N. H. Azimi, X. Hou, H. Gupta, and J. Gao, "Data preservation under spatial failures in sensor networks," in *MOBIHOC*, 2010.

[24] S. P. Borgattia and M. G. Everett, "A graph-theoretic perspective on centrality," *Social Networks*, vol. 28, no. 4, pp. 466–484, October 2006.

[25] T. H. Grubesic, T. C. Matisziw, A. T. Murray, and D. Snediker, "Comparative approaches for assessing network vulnerability," *International Regional Science Review*, vol. 31, no. 1, pp. 88–112, January 2008.

[26] A. T. Murray, T. C. Matisziw, and T. H. Grubesic, "Multimethodological approaches to network vulnerability analysis," *Growth and Change*, vol. 39, no. 4, pp. 573–592, 2008.

[27] R. L. Church, M. P. Scaparra, and R. S. Middleton, "Identifying critical infrastructure the median and covering facility interdiction problems," *Annals of the Association of American Geographers*, vol. 94, no. 3, pp. 491–502, 2004.

[28] D. Goyal and J. J. Caffery, "Partitioning avoidance in mobile ad hoc networks using network survivability concepts," in *7th International Symposium on Computers and Communications*, 2002.

[29] M. Hauspie, J. Carle, and D. Simplot, "Partition detection in mobile ad hoc networks using multiple disjoint paths set," in *Proceedings of 2nd IFIP Mediterranean Ad Hoc Networking Workshop (MED-HOC-NET), Mahdia, Tunisia*, 2003, pp. 25–27.

[30] M. Jorgic, I. Stojmenovic, M. Hauspie, and D. Simplot-ryl, "Localized algorithms for detection of critical nodes and links for connectivity in ad hoc networks," in *Proceedings of 3nd IFIP Mediterranean Ad Hoc Networking Workshop (MED-HOC-NET)*, 2004, pp. 360–371.

[31] T. N. Dinh, Y. Xuan, M. T. Thai, E.K.Park, and T. Znati, "On approximation of new optimization methods for assessing network vulnerability," in *INFOCOM*, 2010.